Bubble-scale model of foam mechanics: Melting, nonlinear behavior, and avalanches

D. J. Durian*
Department of Physics and Astronomy, University of California, Los Angeles, California 90095-1547
(Received 10 September 1996)

By focusing on entire gas bubbles, rather than soap films or vertices, a microscopic model was recently developed for the macroscopic deformation and flow of foam in which dimensionality, energy storage, and dissipation mechanisms, polydispersity, and the gas-liquid ratio all can be varied easily [D. J. Durian, Phys. Rev. Lett. **75**, 4780 (1995)]. Here, a more complete account of the model is presented, along with results for linear rheological properties as a function of the latter two important physical parameters. It is shown that the elastic character vanishes with increasing liquid content in a manner that is consistent with rigidity percolation and that is almost independent of polydispersity. As the melting transition is approached, the bubble motion becomes increasingly nonaffine and the relaxation time scale appears to diverge. Results are also presented for nonlinear behavior at large applied stress, and for the sudden avalanchelike rearrangements of bubbles from one tightly packed configuration to another at small applied strain rates. The distribution of released energy is a power law for small events, but exhibits an exponential cutoff independent of system size. This is in accord with multiple light scattering experiments, but not with other simulations predicting self-organized criticality. [S1063-651X(97)14002-8]

PACS number(s): 82.70.Rr, 83.70.Hq, 05.40.+j

I. INTRODUCTION

Aqueous foams consist of a random dispersion of gas bubbles in a much smaller volume of liquid [1,2]. If the solution contains enough stabilizing surfactants, or other surface-active agents, then the structure formed by the collection of bubbles can be essentially constant over time scales ranging from minutes to hours. One can then reasonably ask about the mechanical, or rheological, properties of the foam as a material. The response of aqueous foams to externally applied forces is striking [3–5]. Even though they consist mainly of gas and relatively little liquid, foams can support small shear forces like an ordinary solid. The origin of this elasticity is in the increase in gas-liquid surface area, and the corresponding energy cost given by the surface tension, as the tightly packed bubbles distort under application of shear. If the applied forces are sufficiently small, then the response is linear and the shear modulus is given by the stress per unit strain whether the experiment is performed under controlled stress or controlled strain conditions. As the applied stress or the imposed strain is gradually increased, the behavior becomes increasingly complex. In the case of applied stress, for example, the response first changes from linear to nonlinear. Next, the response becomes irreversible as topological changes are induced in which a few bubbles in a finite region suddenly change neighbors. As the applied stress is increased further, more and more rearrangements occur but the resulting strain remains finite. Finally, when the applied stress exceeds a ''yield'' stress, the system flows indefinitely at nonzero strain rate by a never-ending series of neighbor-switching rearrangements. If the strain rate is low, the rearrangements are discrete avalanchelike events; but if the strain rate is high the deformation is more homogeneous and continuous, as in a simple viscous liquid.

The purpose of this paper is to explore, via computer simulation, the connection between the complex macroscopic rheological behavior of foams and the underlying microscopic structure and dynamics of the tightly packed gas bubbles. Special attention will be paid to the role of key structural parameters such as gas volume fraction and the bubble size distribution. These issues are of intrinsic interest, not only because the range of behavior is rich and unusual, but also since foams are familiar from everyday life and are useful as materials in a broad range of applications. Study of foams may also shed light on related systems where tight packing of discrete objects is crucial, such as concentrated emulsions and colloids, as well as granular media. Furthermore, theoretical study is especially timely since the advent of multiple-light-scattering techniques is permitting new and as-yet unexplained experimental insights into bubble-scale dynamics [6–11].

Since foams are naturally disordered, and since the bubble rearrangement dynamics are nonlinear and collective, computer simulation is an important tool for theoretical study. Analytical calculation is possible only for periodic systems [5,12,13,37], or for linear rheological features [14]. While such work can provide important insights, it cannot capture the full range of behavior. The first simulations of foam rheology were by Weaire and co-workers for two-dimensional foams with zero liquid content, where the packing of bubbles can be described entirely by the continuous network of thin structureless soap films that separate adjacent bubbles [15,16]. The geometry and topology of this network are highly constrained, as specifically accounted for in Weaire's approach. For instance, the vertices at which films meet are all three-fold coordinated; if a film shrinks to zero length, leaving an unstable fourfold vertex, then a neighbor-switching topological rearrangement is implemented. The only degrees of freedom are the end points and curvature of each film; these are adjusted to minimize total interfacial area for the given topology subject to the constraint that the

*Electronic address: durian@physics.ucla.edu

area of each bubble be fixed and the curvature be constant along each film. This is done in a ''quasistatic'' fashion since dissipation mechanisms are not included; consequently, there are no viscous stresses, and the network structure is always in static mechanical equilibrium [17,18].

For three-dimensional foams, this general program is only now starting to be implemented, largely because description of the network of soap films is significantly more difficult. Geometrically, the soap films have two different radii of curvature that are neither constant nor independent; only the total curvature, and hence Laplace pressure across the interface, is constant. Topologically, the only stable junction of films is threefold coordinated, and these so-called Plateau borders are curves that are not necessarily confined to a plane; the only stable junction of Plateau borders is fourfold coordinated. Yet another difficulty is that foams in nature usually contain enough liquid that the vertices, Plateau borders, and films all develop further structure that cannot be ignored. It is proving possible to account for some of this complexity by using the surface evolver program developed by Brakke [19]. Such efforts have concentrated on dry periodic systems [20,21], though randomness and nonzero liquid content are being pursued [22]. As in Weaire's original approach, this is restricted to static phenomena since dissipation effects cannot be included.

For two-dimensional foams, Weaire's group has made significant progress in accounting for the effects of nonzero liquid content [23–27]. This permits study of how the striking elastic character vanishes, or melts, as the liquid content is increased and the bubbles become able to translate, rather than distort, in response to imposed strain. Incorporation of liquid is achieved by decorating the Plateau borders at which three films meet with a small amount of liquid and by using Laplace's law to insure that the pressure is the same throughout all borders and uniform within each bubble. Further approximations, besides quasistatic dynamics, are (1) the soap films are structureless and straight outside the Plateau borders, which implies that the pressure is incorrectly the same inside each bubble, and (2) liquid is not conserved but rather is created locally as needed in order to satisfy Laplace's law. Perhaps because of such approximations, this approach breaks down for foams wetter than about 89% gas content and precludes definitive quantitative study of the melting transition near 84% gas content.

In a separate effort, important advances have also been made recently by Kawasaki and co-workers in accounting for the effects of realistic dissipation mechanisms in dry two-dimensional foams [28–30]. This permits simulation of shear at nonzero rates and of the transition from plastic to fluid behavior as the shear rate is increased. Of the many possible dissipation mechanisms [31–33], the dominant one for dry foams is shear flow of the infinitesimal amount of viscous liquid within the Plateau borders as a film is stretched or shrunk [34]. To incorporate this mechanism most readily, the films are approximated as straight line segments. Equations of motion are then generated for the Plateau borders where three films meet by balancing dissipation forces with surface tension forces according to Newton's second law for a massless object. These are then solved subject to the constraint that each bubble has constant area, and with suitable rules for topology change when a film shrinks to zero length. This is called the ''vertex'' model [28–30], since the Plateau borders in a two-dimensional dry foam are structureless points. Since ''vertices'' are the fundamental structural unit in this approach, it is not applicable either for foams with nonzero liquid content or for foams in three dimensions.

The models described above are all either at, or are essentially expansions about, the dry foam limit where gas bubbles are nearly polyhedra separated by thin curved soap films. All are based on different uncontrolled approximations and have different limited ranges of applicability. This makes it nearly impossible to reconcile conflicting predictions, as, for instance, in the case of the avalanchelike rearrangements to be discussed later. Furthermore, none alone is able to capture the full range of behavior seen in nature. Perceiving the need for a simpler, more all-encompassing framework for considering how disorder, dimensionality, and microscopic phenomena individually influence foam rheology, I recently introduced a ''bubble'' model based on a physical picture of pairwise interactions between entire gas bubbles [35]. It is essentially an expansion about the wet foam limit, where the gas bubbles are nearly d-dimensional spheres that are hence simple to describe. As do the previous models, this approach also rests upon uncontrolled approximations; however, its parameters can be varied much more widely. In particular, it has the unique advantage of simultaneously incorporating interaction and *dissipation* effects for foams of arbitrary *disorder*, *liquid content*, and *dimensionality*. Its most serious flaw is that it does not explicitly account for bubble shapes and liquid degrees of freedom, and hence does not possess a dry foam limit where the osmotic pressure diverges to maintain the gas fraction below one. Otherwise, the bubble model successfully reproduces the known qualitative features of static and dynamic foam rheology, in many instances quantitatively [35,36]. Therefore, this approach provides an important complement to the previous models and can serve as a basis for developing physical intuition about the particular influence of various microscopic ingredients, for exploring new phenomena, and for reconciling the other simulations approaches with each other and with experiment. Here, I will first recapitulate more fully the construction and implementation of the bubble model and then present new results for the influence of polydispersity on the melting transition and for the nonlinear behavior at finite stress levels and strain rates.

II. BUBBLE MODEL

In a very wet foam, the gas bubbles are all spherical and the only structural quantities are their radii $\{R_i\}$ and the time-dependent position vectors $\{\vec{r}_i\}$ of their centers. The immediate goal is to develop equations of motion for the $\{\vec{r}_i\}$ by considering all the pairwise interactions between neighboring gas bubbles. No explicit degrees of freedom will be included for bubble shapes or for flow within the continuous liquid phase. Physically, then, imagine what occurs if two actual gas bubbles are gradually brought into contact at infinitesimal rate in an otherwise empty sea of liquid. Both bubbles will remain spherical and experience no forces until essentially touching, since the ranges of the van der Waals force (attractive, originating from the dielectric mismatch between gas and liquid) and of the electric double-layer force

(repulsive, originating from the adsorbed surfactants) are typically less than 100 nm, which is much less than the typical gas bubble size of more than 20 μm. If pushed into geometrical contact, such that the center-to-center distance is less than the sum of their radii, the two gas bubbles will distort in shape rather than coalesce. The region of contact will then flatten out into a soap film with a thickness determined by the combination of applied, van der Waals, and double-layer forces. This and the concomitant increase in total surface area give rise to a mutually repulsive force proportional to the gas-liquid surface tension, σ_{gl}. This repulsive force is nearly harmonic [25,36–39], that is, proportional to the size of the deformation $\xi=(R_i+R_j)-|\vec{r}_i-\vec{r}_j|$. In two dimensions this is an excellent approximation. In three dimensions, numerical calculation of the detailed bubble shapes shows that the interaction potential rises approximately as ξ^{α}, where α ranges from 2.1 to 2.6, depending on the bubble coordination number, which is slightly faster than harmonic [36,39].

For simulations of the bubble model presented earlier [35] and to be carried further here, the repulsive force is taken to be perfectly harmonic as follows. The effective spring force for each bubble scales as the Laplace pressure, σ_{gl}/R_i, since large bubbles are more easily deformed. For two mutually repulsing bubbles, $|\vec{r}_i-\vec{r}_j|<(R_i+R_j)$, the individual springs are added in series such that the effective spring constant is $F_0/(R_i+R_j)$; physically, the force constant F_0 plays the role of surface tension but with units of force; for a real foam it would be on the order of $F_0\cong\sigma_{gl}\langle R\rangle$, where $\langle R\rangle$ is the average bubble radius.. The repulsive force $\vec{F}^r_{ij}$ acting on the center of bubble i due to bubble j is then given by the spring constant multiplied by the compression and a unit vector:

$$\vec{F}^r_{ij}=\frac{F_0}{(R_i+R_j)}\left[(R_i+R_j)-|\vec{r}_i-\vec{r}_j|\right]\frac{(\vec{r}_i-\vec{r}_j)}{|\vec{r}_i-\vec{r}_j|}$$
$$=F_0\left[\frac{1}{|\vec{r}_i-\vec{r}_j|}-\frac{1}{(R_i+R_j)}\right](\vec{r}_i-\vec{r}_j). \quad (1)$$

This force is taken to be strictly repulsive; if the two bubbles do not overlap, then $\vec{F}^r_{ij}$ is set to zero.

The second key ingredient in the bubble model is dissipation. When a foam is strained at nonzero rate, energy is dissipated due to shear flow of the viscous liquid within the soap films and Plateau borders, by flow within the adsorbed surfactants films, and by a variety of other such mechanisms [33]. The simplest assumption, given a description of foam structure entirely by bubble positions and radii, is that this produces a drag force on bubble i from neighboring bubble j in proportion to their velocity difference:

$$\vec{F}^v_{ij}=-b(\vec{v}_i-\vec{v}_j). \quad (2)$$

The proportionality constant b is assumed to be the same for all pairs of bubbles. To see that this is reasonable, consider an actual foam where the bubbles are packed together such that their shapes are all of comparable distortion away from spherical. The intervening soap films are similarly all of comparable area, of order $\langle R\rangle^2$ as set by the typical bubble size, and of comparable thickness l as set by the liquid content and the competition of surface tension and interaction forces. When two interacting bubbles move with speed V relative to one another, the viscous liquid within the intervening soap film remains of roughly fixed thickness and is sheared at rate V/l. The drag force per unit area then has magnitude $F^v_{ij}/\langle R\rangle^2=\eta V/l$, where η is the liquid viscosity. This shows that Eq. (2) has the proper form if shear within the films is the dominant dissipation mechanism, and gives an estimate for the constant as $b=\eta\langle R\rangle^2/l$.

To find the time evolution of the center position of bubble i, the contributions of Eqs. (1) and (2) for the repulsive and drag forces must simply be summed over all the neighboring bubbles j. Since inertial effects are negligible, this total force must add to zero according to Newton's second law. Simplifying for the velocity of bubble i gives the following equation of motion:

$$\vec{v}_i=\langle\vec{v}_j\rangle+\frac{F_0}{b}\sum_j\left[\frac{1}{|\vec{r}_i-\vec{r}_j|}-\frac{1}{R_i+R_j}\right](\vec{r}_i-\vec{r}_j)+\frac{\vec{F}^a_i}{b}, \quad (3)$$

where only neighboring bubbles contribute to the average velocity $\langle\vec{v}_j\rangle$ and the sum of repulsive forces. If bubble i is an edge bubble, then an applied force $\vec{F}^a_i$ may be imposed with normal and tangential components that, respectively, give the local pressure and shear stress, as would be transmitted from a wall. Bubble motion will be generated strictly according to Eq. (3) throughout this paper, though useful variations can be made to details of the viscous and repulsive [36] ingredients. This simple, physically motivated model has several key advantages over previous approaches. First, since Eq. (3) is a vector equation, it can be implemented easily in any number d of spatial dimensions keeping all other ingredients constant. By contrast, prior simulations were all based on dimension-specific topological features of the bubble-packing structure. Second, the gas-liquid volume fraction can be varied arbitrarily over the entire range $0<\phi<1$ simply through choice of size and number of bubbles per unit volume. By contrast, prior simulations were all based on approximate decoration of the topological structure, and have been restricted to relatively high gas fractions, well above the melting point. And third, stress relaxation can be studied and the strain rate can be varied. By contrast, prior simulations were all either quasistatic, or else intrinsically limited to two-dimensional foams with gas fraction of identically one. The bubble model of foam rheology represented by Eq. (3) is the first in which the effects of randomness, dimensionality, liquid content, and microscopic interaction and dissipation effects can all be accounted for and systematically explored.

One important consequence immediately apparent from Eq. (3) is that bubble motion is highly overdamped. Furthermore, for a given set of bubbles, the only parameter affecting this dynamics is a microscopic time scale, $\tau_d=b\langle R\rangle/F_0$, set by the average bubble size and the competition between mechanisms for storing and dissipating energy. The individual values of b and F_0 are not relevant. Physically, τ_d represents the exponential relaxation time constant for motion of a typical bubble toward equilibrium while all other bubbles are held fixed, and thus gives the shortest time scale for the *duration* of a topological rearrangement event. Of course, as will be discussed in detail later, collective effects

involving the simultaneous motion of many bubbles can cause complete relaxation to last significantly longer; the ultimate relaxation time may even depend on system size. Even though Eqs. (1) and (2) merely approximate the true effects of surface tension and viscosity, respectively, and even though other storage and dissipation mechanisms may be important, Eq. (3) should reasonably be expected to capture the essential behavior since there will always be a characteristic microscopic time scale and since the dynamics will always be overdamped. It is thus to be hoped that the general approach of the bubble model has applicability beyond the assumptions made in its derivation.

III. SIMULATION DETAILS

It is straightforward to integrate numerically the equations of motion in Eq. (3) to find the response of a given system of bubbles to various applied forces. Before results are presented in the next several sections, I first outline common technical details for how systems are actually chosen, how forces are applied, and how the numerical integration is performed.

As in the previous simulations [35], the results presented here are all for two-dimensional $N\times N$ systems of bubbles confined to a square of edge length L. The top-N and bottom-N edge bubbles are held at fixed height and relative positions, as though stuck to movable plates, while periodic boundary conditions are imposed to the left and right. The bubble radii are taken from a triangular distribution that peaks at $\langle R\rangle$ and vanishes at $(1\pm w)\langle R\rangle$. To investigate the effects of polydispersity, the width w of the distribution is set either to $w=0.75$, for a polydisperse size distribution similar to that which naturally arises from coarsening by gas diffusion, or $w=0.10$, for a more monodisperse foam as may be specially constructed. With such a distribution, the average bubble area is $\langle A\rangle=\pi\langle R\rangle^2[1+w^2/6]$ and the gas volume fraction is given by the total bubble area, ignoring overlaps, as $\phi=N^2\langle A\rangle/L^2=\pi N^2\langle R/L\rangle^2[1+w^2/6]$. The value of $\langle R\rangle$ is thereby chosen in units of the system edge length according to the desired gas fraction. Bubble radii are then drawn randomly from this distribution, and the very last one is chosen such that the gas fraction is identically as specified. If this last, required, radius lies outside the triangular distribution, or if the width of the realized set of bubbles is off by more than 0.1%, then another set is drawn. This procedure is employed separately for bubbles along both top and bottom edges, as well as in the bulk.

Before rheology simulations can begin, the chosen system of bubbles must first be equilibrated. This is done in two separate tasks. The first is to construct rigid walls from the N top and N bottom edge bubbles. These bubbles are initially spread evenly along straight lines, to which they will be forever confined. Their positions along the lines are then repeatedly updated according to the equation of motion, Eq. (3), until the total force on each bubble from the sum of its two edge neighbors is zero. Both the applied force and the average neighbor velocity terms in Eq. (3) are set to zero; the latter is required to break translational symmetry and damp out the motion. After this is accomplished, the relative positions of the edge bubbles are held fixed in order to form rigid walls that may be slid with respect to one another and thereby shear the intervening bubbles. The second equilibration process is to relax the N^2-2N bulk bubbles, initially placed on a triangular lattice, with respect to both each other and also the top and bottom walls. It is crucial that this be done carefully in order to observe linear rheological behavior, where the shear modulus, for example, is independent of the sign and magnitude of the strain. At successive time steps, the position of each bulk bubble is adjusted according to Eq. (3) from the repulsive spring forces it experiences from all its neighbors, both in the bulk and within the top or bottom walls. As in the first equilibration process, the applied force and average neighbor velocity terms are set to zero. Also at each time step, the top and bottom edge bubbles are slid as a rigid unit according to the parallel component of the total repulsive spring forces exerted from all the neighboring bulk bubbles. This is repeated until the total force on each bulk bubble, and the total lateral force on the top and on the bottom walls, are all zero.

Standard techniques are employed in order to make both the equilibration and the subsequent rheology simulations efficient and accurate. First, instead of comparing each bubble with all others to determine the existence of a spring force, only fairly close neighbors are examined by means of a linked list [40]. This reduces the number of pairs of bubbles to be compared at each time step from order N^2 to order N. Second, instead of employing a forward (Euler) finite differencing scheme to generate the change in bubble positions in a time interval Δt, $\vec{r}_i(t+\Delta t)=\vec{r}_i(t)+\vec{v}_i(t)\Delta t$, where $\vec{v}_i(t)$ is given explicitly by the right-hand side of Eq. (3), a semi-implicit scheme is used in which steps are generated from information that is more symmetrical across the time interval (Ref. [41], Chap. 15). In particular, new positions are taken as $\vec{r}_i(t+\Delta t)=\vec{r}_i(t)+\frac{1}{2}[\vec{v}_i(t)+\vec{v}_i(t+\Delta t)]\Delta t$, where $\vec{v}_i(t+\Delta t)$ is estimated in terms of positions and velocities at time t from the matrix of partial derivatives of the right-hand side of Eq. (3) with respect to positions. This permits the time step to be made as large as $\Delta t=0.2\tau_d$ without noticeably affecting the results. By contrast, the Euler scheme is unstable and requires that Δt be infinitesimal in terms of τ_d.

One final point is that for all the simulation results presented here and in Ref. [35], the average velocity term in the right-hand side of Eq. (3) is taken as $\langle\vec{v}_j\rangle=\dot{\gamma}y_i\hat{x}$, where $\dot{\gamma}$ is the imposed shear strain rate, y_i is the coordinate of bubble i, and $\hat{x}$ is the unit vector in the imposed flow direction. This is done mainly for computational simplicity, since then the right-hand side of Eq. (3) gives the velocity of each bubble i exclusively in terms of the bubble positions, but has other benefits as well. Taking $\langle\vec{v}_j\rangle$ as a literal average would require that the equations of motion for all bubbles be simultaneously solved for the bubble velocities prior to integration; this entails the inversion of a large sparse matrix at each time step, and also significantly complicates the use of implicit finite differencing. However, note that $\langle\vec{v}_j\rangle=\dot{\gamma}y_i\hat{x}$ is actually a reasonable approximation if the typical bubble coordination number is very large. Furthermore, it is the correct description of the viscous interaction of an isolated bubble in a viscous liquid undergoing shear, and is therefore superior to a literal average in the limit of small gas area fraction.

Whatever its pros and cons, the choice adopted here for

$\langle \vec{v}_j \rangle$ cannot affect equilibrium configurations or static elastic properties. It can, however, affect other phenomena to be studied here such as bubble dynamics under steady shear and stress relaxation following step strain. Work is now in progress [42] that will examine empirically the sensitivity to details of the interactions assumed in Eq. (3). Until this is completed, some insight can be gained by treatment of a one-dimensional, periodic version of the bubble model. Consider, then, a chain of massless beads connected by springs, each with force constant k. The equations of motion for the bead positions, x_n, can be written as

$$0 = k[x_{n+1} + x_{n-1} - 2x_n] + \beta_1[\dot{x}_{n+1} + \dot{x}_{n-1} - 2\dot{x}_n] - \beta_2 \dot{x}_n \tag{4}$$

where two terms involving time derivatives represent two distinct viscous interactions. In the context of foams, the β_1 term represents dissipation due to relative motion of adjacent bubbles as caused, for example, by shear of the intervening liquid. This corresponds to a literal computation of $\langle \vec{v}_j \rangle$ in Eq. (3), which would not vanish during relaxation. The β_2 term represents dissipation due to absolute motion of bubbles with respect to the continuous fluid phase, as happens, for example, at very low gas fractions or during relaxation from a state with more fluid on one side of the sample than the other. This corresponds to the choice $\langle \vec{v}_j \rangle = \dot{\gamma} y_i \hat{x}$ adopted here for Eq. (3), which vanishes during relaxation. For the periodic one-dimensional model, the relaxation spectrum can be found easily keeping both terms. Modes of wave vector κ relax exponentially as $\exp(-\omega\tau)$, where

$$\omega(\kappa) = k(1 - \cos\kappa a)/[\beta_1(1 - \cos\kappa a) + \tfrac{1}{2}\beta_2] \tag{5}$$

and a is the equilibrium bead separation. For the special case $\beta_2 = 0$, all modes relax at the same rate, $\omega(\kappa) = k/\beta_1$. In general, however, the fastest modes are at short wavelengths, $\kappa a \cong \pi/2$, and relax with rate $\omega(\kappa) \cong k/(\beta_1 + \frac{1}{2}\beta_2)$, whereas the slowest modes are at long wavelengths, $\kappa a \ll 1$, and relax with rate $\omega(\kappa) \cong k(\kappa a)^2/\beta_2$ independent of β_1. The longest possible relaxation time thus varies with the square of the system size. Such length-scale-dependent dynamics may be expected for a real foam, where the collective relaxation of bubble shapes is accompanied by the flow of liquid throughout the entire interconnected porous geometry between the tightly packed bubbles. The β_2 term, corresponding to the choice $\langle \vec{v}_j \rangle = \dot{\gamma} y_i \hat{x}$ adopted here for simulations using Eq. (3), is needed to capture this behavior.

IV. STEP-STRAIN RESULTS

In this section, results are given for the linear response of two-dimensional square samples of $N \times N$ bubbles subjected to a step strain. Attention will be restricted to $N = 20$ since previous work [35] showed this to be sufficiently large that the variance between different realizations of bubbles does not obscure trends.

A. Stress relaxation

After thorough equilibration, the rheology simulations begin with the instantaneous imposition of an affine step strain, of size γ, in which the x coordinate of each bubble center is shifted to $x + \gamma y$. Note that such a deformation is consistent with Eq. (3) for brief application of shear at a very large shear rate $\dot{\gamma}$, where the viscous forces completely dominate the repulsive spring forces. Next, the bulk bubbles are allowed to move according to Eq. (3), with $\langle \vec{v}_j \rangle = \dot{\gamma} y_i \hat{x} = 0$, until mechanical equilibrium is achieved, all the while keeping the edge bubbles fixed. This relaxation process is monitored via the total energy stored in the springs and the total shear stress on the walls. The total energy is defined as the sum over all pairs of interacting bubbles as one-half of the spring constant times the square of the compression; the shear stress σ is defined as the average lateral force per edge bubble. Typical results for a step strain of $\gamma = 10^{-5}$ are shown in Fig. 1 for four configurations of bubbles with gas fractions of $\phi = 1$ (dry) and $\phi = 0.84$ (wet) and with triangular size distributions of widths $w = 0.75$ (polydisperse) and $w = 0.10$ (monodisperse). The top plot in Fig. 1 displays the difference in energy from the final value normalized so that the decay starts at one. The data all exhibit nonexponential relaxations that span many decades in time ranging from about 1% at $0.01\tau_d$ to full decay at $(200\text{–}5000)\tau_d$, consistent with the presence of many length-scale-dependent relaxation times predicted by the periodic one-dimensional version of the model. The bottom plot in Fig. 1 displays the stress relaxation divided by the magnitude of the imposed step strain. These data all exhibit nonexponential relaxations, as for the energy, but that are not necessarily monotonic due to the choice $\langle \vec{v}_j \rangle = \dot{\gamma} y_i \hat{x} = 0$. The final value for the decay is nonzero, since the system is strained, and gives the shear modulus as $G = \lim_{\tau \to \infty} \sigma(\tau)/\gamma$. Note that G is greater for the dry foams and that the total relaxation time is greater for the wet foams, independent of polydispersity. For all the examples given here, the response is linear in that G is independent of strain, and no new springs are formed or existing springs broken, for step strains up to roughly $|\gamma| < 10^{-3}$.

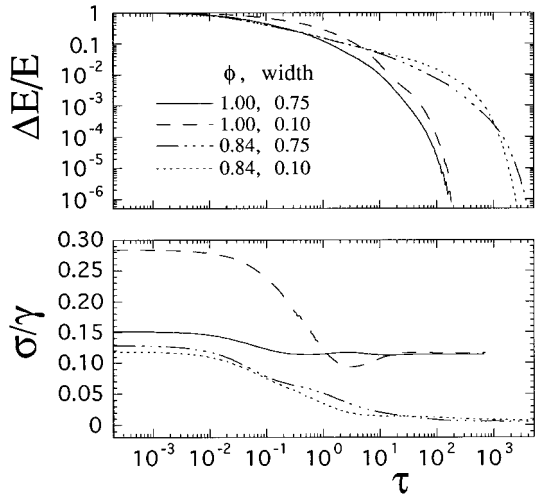

FIG. 1. Energy and stress relaxation as a function of time following an imposed step strain of $\gamma = 10^{-5}$ for four 20×20 systems of bubbles. The different line codes indicate gas fraction ϕ and the relative width of the bubble size distribution as labeled.

The equilibrium bubble configurations for the four particular foams just discussed are shown two ways in the next figures. Figure 2 displays both the bubbles, as dotted circles,

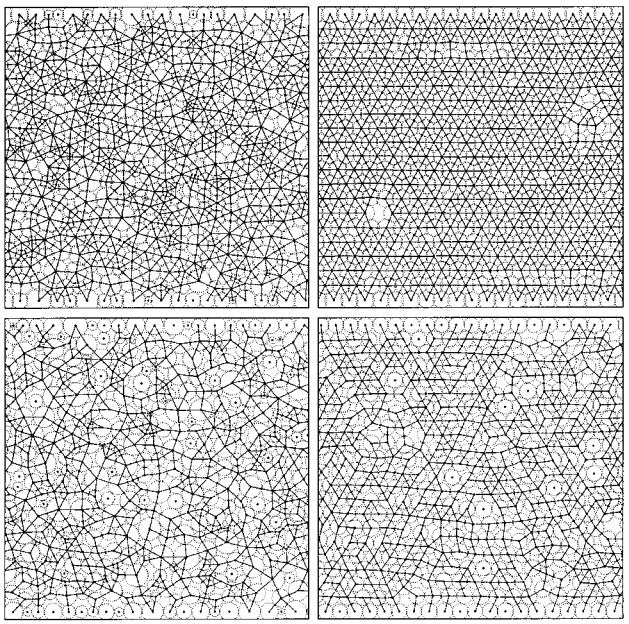

FIG. 2. Equilibrium bubble configurations for the four systems examined in Fig. 1. The top two and bottom two have gas fractions of $\phi=1.0$ and 0.84, respectively; the left two and right two have distribution widths of $w=0.75$ and 0.10, respectively. Note that the top and bottom edge bubbles are fixed to a horizontal plate, while periodic boundary conditions are imposed to the left and right. A solid line is drawn between the centers of adjacent bubbles if they overlap and hence, physically, repel one another by a spring force. These repulsive spring networks percolate across the system and give the foam shear rigidity.

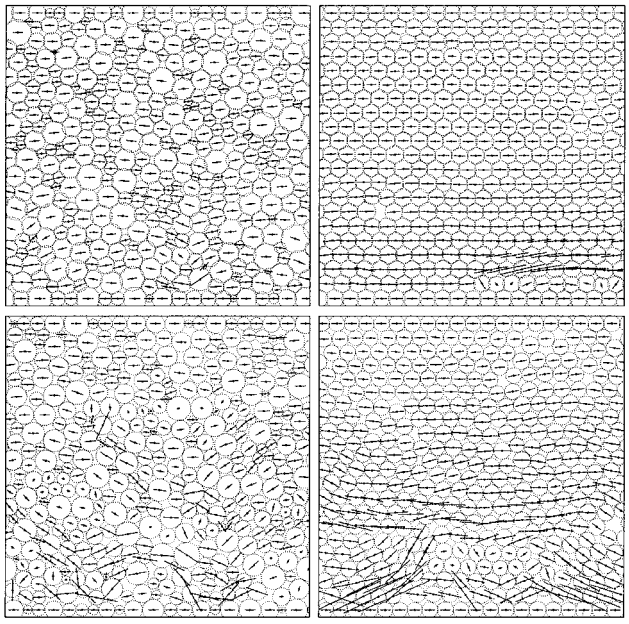

FIG. 3. The same configuration of bubbles shown in Fig. 2, now with lines through the centers that depict the direction and magnitude of motion during relaxation after an imposed step strain as described in the text. This motion becomes increasingly nonaffine for greater liquid content and polydispersity.

and the spring network, as solid lines between the centers of pairs of repulsing bubbles. A spring is thus drawn only when the circles representing two bubbles happen to overlap, where actual bubbles would distort in shape away from spherical and hence repel each other. The overlaps are large enough to be visible in Fig. 2 only for the dry foams. Note that by contrast with other studies of random spring networks, the springs shown in Fig. 2 are all compressed; none is stretched. Inspection shows that the networks are sparser for the wetter foams, as expected, since bubbles are then on average further apart and interact with fewer nearest neighbors. In fact, all bubbles are involved in the network for the dry foams, but occasional isolated bubbles occur in the wet foams. In both cases, the networks of compressed springs in Fig. 2 all percolate not just from top to bottom, as required to support static shear, but across the entire sample. Another feature apparent in Fig. 2 is that the networks are more ordered for monodisperse foams, since in two dimensions identical spheres tend to crystallize when packed. The wet monodisperse foam is not as highly ordered as the dry since its bubbles are only barely packed together.

The motion of bubbles that occurs during relaxation following sudden step strain is shown next in Fig. 3, for the same four foams. Both the magnitude and direction of the motion are indicated by a small line segment through the center of each bubble given by $(\vec{r}_i-\vec{r}_i^{\,e})/\gamma y_i$ times a constant; $\vec{r}_i$ is the new position of bubble i after stress relaxation, $\vec{r}_i^{\,e}$ is its equilibrium position before the step strain was imposed, and the scaling constant is chosen so that the average segment size is smaller than the average bubble diameter. According to this scheme, regions within the foam that undergo affine shear deformation, $(x_i,y_i)\rightarrow(x_i+\gamma y_i,y_i)$, such as in the edge bubbles of Fig. 3 or in a periodic network free of defects, therefore all have horizontal line segments of equal size. The response of bulk bubbles thus displayed in Fig. 3 is evidently neither homogeneous nor affine. Nevertheless, large correlated regions in which the motion is nearly affine exist, inside of which the line segments are all of comparable size and direction. The trend apparent in Fig. 3 is that these uniformly elastic regions are more prevalent for drier more monodisperse foams. The motion is least affine for the wet polydisperse foam, where the size and direction of the line segments are the least spatially correlated and can, in fact, vary wildly between neighboring bubbles.

The line segments displayed in Fig. 3, depicting how stress is relaxed following step strain, allow visualization of the motion that would occur in linear response to oscillatory strain. If sinusoidal strain is imposed at a frequency ω that is small in comparison with the reciprocal of the longest relaxation time, τ_r, as seen Fig. 1, then viscous forces can be neglected and the spring forces on each bubble will sum to zero throughout the entire strain cycle. The motion is hence quasistatic, and each bubble will move sinusoidally with amplitude and direction prescribed by the line segments in Fig. 3. As the oscillation frequency increases, however, the viscous forces will become more important, and the bubble motion will eventually become affine in the limit $\omega\gg\tau_r^{-1}$.

The line segments in Fig. 3 also support a recent model for the anomalous viscous dissipation observed in three-dimensional, random, monodisperse emulsions [14]. There, an extra $\sqrt{i\omega}$ contribution to the complex dynamic shear modulus, $G^*(\omega)$, was observed and attributed to a distribution of ''weak'' regions in which bubbles can shift their rela-

tive positions rather than distort elastically. These shifts are proposed to occur where several bubbles are packed together in such a way that they can be sheared in certain ''easy'' directions with a smaller elastic penalty than in others. The $\sqrt{i\omega}$ contribution then arises, in both two and three dimensions, from the fact that mechanical energy is dissipated, rather than stored, in regions where bubbles shift and from the assumption that the sample is isotropic on average, even though it is locally anisotropic due to the presence of easy directions. The simulation data in Fig. 3 are consistent with this picture. Areas in which the deformation is roughly affine can be identified as the ''strong'' regions, where energy is predominantly stored; and areas where the deformation is especially inhomogeneous can be identified as the ''weak'' regions, where energy is predominantly dissipated. Furthermore, the relaxation results in Fig. 1 may also be consistent with this model and the emulsion experiments. Since the complex dynamic shear modulus and the stress relaxation modulus are related by Fourier transform, a $\sqrt{i\omega}$ contribution to $G^*(\omega)$ corresponds to $1/\sqrt{\tau}$ behavior in the stress relaxation. This is consistent with the gradual relaxation observed in Fig. 1, and the fact that the exponential cutoff moves out for larger systems [35]. Further simulations are required both to test decisively the model of Liu *et al.* and to distinguish the relative importance of the random packing geometry from the choice of viscous dynamics in Eq. (3) on the gradual stress relaxation.

B. Melting transition

Consider now the trends in linear rheological properties as a function of liquid content. In particular, consider the nature of the melting transition as the liquid content is increased and the bubbles become free to move around one another without any elastic distortion. This transition is tracked four ways in Fig. 4 for sequences of polydisperse (width $w=0.75$) and monodisperse ($w=0.10$) foams subjected to instantaneous step strains of magnitude $\gamma=10^{-5}$. The four quantities displayed as a function of gas fraction ϕ are the shear modulus G, the average normal force per edge bubble or pressure P, the coordination number, or mean number of spring forces per bulk bubble Z, and the relaxation time τ_r, defined here as the time constant for the final exponential relaxation of the total spring energy following step strain, as seen, for example, in Fig. 1. Before examining the meaning of these data, first note that an entirely new realization of bubbles is constructed for each gas fraction. The scatter in the four quantities shown in Fig. 4 is therefore purely statistical, and is much greater than the accuracy with which any of these quantities is determined for a given realization; indeed, the results in Ref. [35] showed how the scatter from realization to realization decreases as a function of system size. This approach is more time consuming, but avoids introducing systematic artifacts in the quantitative ϕ dependence of rheological parameters that would result if, instead, the gas fraction were adjusted more simply by scaling the radii of all the bubbles in a single configuration. Also, note that there is no dry foam limit as the gas fraction approaches 1. There, in a real foam, the pressure should diverge [43,26,39] and the shear modulus should reach its limiting value with zero slope [24,25,27]. The behavior of the bubble model near $\phi=1$ is

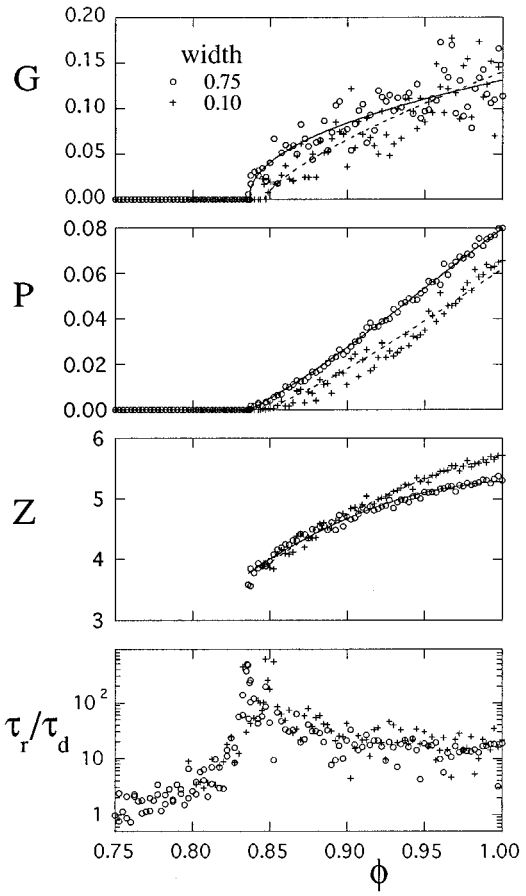

FIG. 4. The melting of polydisperse (width $w=0.75$) and monodisperse ($w=0.10$) foams vs gas fraction ϕ. The static shear modulus G, pressure P, and coordination number (average number of spring contacts per bubble) Z, all vanish, while the stress relaxation time τ_r diverges, at about $\phi=0.84$. Each point represents an entirely different 20×20 realization of bubbles.

therefore not indicative of very dry foams, but rather of more typical ones with greater, nonzero liquid content.

Outside the dry foam regime, consider the results in Fig. 4 for the static quantities, G, P, and Z as a function of ϕ. These all decrease as the liquid content is increased, and simultaneously vanish below a critical gas fraction that depends slightly on polydispersity, $\phi_c=0.835\pm0.005$ for $w=0.75$, and $\phi_c=0.845\pm0.005$ for $w=0.10$. The simulation approach based on approximate decoration of Plateau borders gives roughly the same critical gas fraction, $\phi_c=0.84$ in Refs. [23, 25, 27] and most recently $\phi_c=0.82$ in Ref. [26], by extrapolation from data for $\phi>\phi_c+0.05$. Here, since data are obtained on both sides of the transition, extrapolation is unnecessary and the uncertainty in ϕ_c is set only by statistical scatter from different bubble configurations. Dense random packings of hard disks with a wide variety of size distributions [44] also give the same critical fraction, $\phi_c=0.84\pm0.01$; furthermore, they give a mean coordination number of $Z_c=3.75\pm0.10$ that is identical to the simulation results displayed in Fig. 4. Note that this coordination number is defined by bubble-bubble contacts, not by a Voronoi construction of nearest neighbors.

Empirically, the increase of G above the melting transition can be described as a power law, $G\propto(\phi-\phi_c)^{\theta}$, where

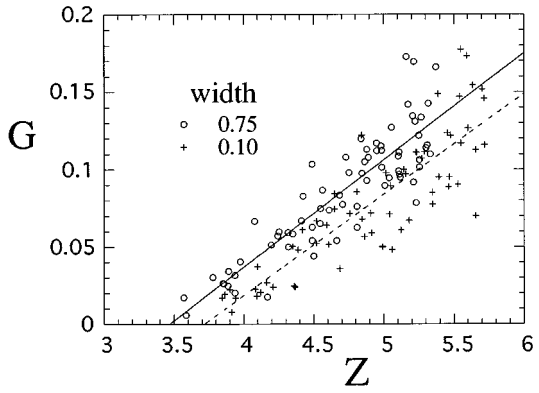

FIG. 5. Shear modulus vs coordination number. The data of Fig. 4, thus replotted, show a linear relationship supporting the rigidity percolation picture of melting.

the exponent is less than 1 but depends noticeably on polydispersity, $\theta=0.5\pm0.1$ for $w=0.75$, and $\theta=0.7\pm0.2$ for $w=0.10$. These power-law fits are shown as the solid and dashed curves, respectively, and are based on data spanning one decade in $(\phi-\phi_c)$. This contrasts with experiments on three-dimensional, random, monodisperse emulsions [38], where G rises almost linearly in $(\phi-\phi_c)$. Based on a variation of the repulsive force law in Eq. (3) according to numerical calculation of bubble shapes, such behavior was attributed in Ref. [36] to disorder plus anharmonicity. However, the increase of θ found here for decreasing polydispersity suggests that details of the narrow size distribution in the emulsion experiments may also play a role.

The quantitative increase of both G and P above ϕ_c can be understood in terms of the ϕ dependence of the coordination number. Physically, the pressure must be proportional to both the average number of spring contacts per bubble and their average compression, and must thus scale as $P\propto Z(\phi-\phi_c)$. Indeed, this form provides an excellent description, independent of polydispersity, as shown by the solid and dashed curves through the pressure data in Fig. 4. This gives a linear increase with $\phi-\phi_c$, in agreement with exact calculation for periodic systems [43,39]. The behavior of the shear modulus cannot be explained by a similarly simple argument. The crucial observation, shown in Fig. 5, is that to within statistical uncertainty G is proportional to $Z-Z_c$ over the entire range. Such behavior is observed in two-dimensional percolation phenomena [45], and supports the contention first made in Ref. [23] that the melting of foams is an example of rigidity percolation. In the usual percolation problem, springs in a random network are progressively cut until rigidity is lost. Here, by contrast, springs are effectively lost with increasing liquid content as pairs of bubbles are given room to push each other apart. The difference is that the topology of the usual random spring network is fixed and the springs may be stretched as well as compressed, whereas here, the springs represent bubble-bubble repulsion, and so cannot be stretched. Furthermore, the network of compressed springs is not fixed but is rather determined by minimizing the total spring energies according to the equation of motion of Eq. (3). If the percolation picture holds, then the repulsive spring networks should become increasingly fractal on approach to the melting transition. While the networks shown in Fig. 2 certainly become sparser near ϕ_c, the system sizes are far too small for a serious test of fractal character. In any case, the simulation results presented here show that the coordination number plays a central role in determining the static elastic properties of foams, independent of polydispersity.

Now that statics have been addressed, consider the results in Fig. 4 for the stress relaxation time τ_r as a function of volume fraction. While the shear modulus and pressure both vanish at ϕ_c, the relaxation time reaches a maximum, rising sharply as the transition is approached from either above or below. This behavior is seen for both the polydisperse and monodisperse systems. Presumably, τ_r would actually diverge at ϕ_c for arbitrarily large samples. This suggests the presence of a diverging length scale, and is thus further consistent with the rigidity percolation picture where the correlation length, beyond which the spring network is homogeneous and below which it is fractal, grows as the transition is approached. This also shows how the transition may be difficult to observe experimentally, both because the time scales become long and because the nature of the rheology is not markedly different on the two sides of the transition. Above, it is a viscoplastic solid with infinitesimal shear modulus; below, it is a viscoelastic liquid with zero shear modulus; on both sides, the transient storage of elastic energy is very long lived and dominates the behavior.

V. CONSTANT STRESS RESULTS

While Sec. IV dealt with linear response as a function of liquid content, this section and the next deal, respectively, with nonlinear behavior at large strain amplitudes and during flow. An alternative approach to static rheology is to consider the strain produced by a given applied stress, as opposed earlier to finding the stress required to support a given imposed step strain. After thorough equilibration, the simulations now begin with the application of a very small shear stress to the bubbles within the top and bottom edge plates. The bulk bubbles are then allowed to move according to Eq. (3) with $\langle\vec{\nu}_j\rangle=0$, and the edge plates are allowed to move independently as a rigid unit according to the sum of applied and spring forces from neighboring bulk bubbles. Eventually, the resulting strain becomes large enough that the total applied force is balanced by the shear elasticity of the system; when all motion stops, the final strain is recorded. The applied stress is then increased slightly and the process is repeated. Simulation results for two such runs are displayed in Fig. 6, both for the same 12×12 system of bubbles with gas fraction $\phi=1$, but with shear forces applied in opposite directions. Raw data are displayed in the inset, and the applied stress divided by resulting strain, σ/γ, are displayed in the main plot. Figure 6, first of all, demonstrates that σ/γ is constant at sufficiently small applied stress, independent of sign. This is the regime of linear response characterized by a shear modulus, $G=\lim_{\sigma\to0}\sigma/\gamma$.

As the applied stress is steadily incremented, the response eventually becomes nonlinear, and then irreversible but still static; for even greater applied stress, continuous flow can occur. Figure 6 shows that the linear regime lasts up to about $|\gamma|\approx10^{-3}$, beyond which σ/γ rises above the value of G. In spite of this nonlinearity, mechanical equilibrium at all

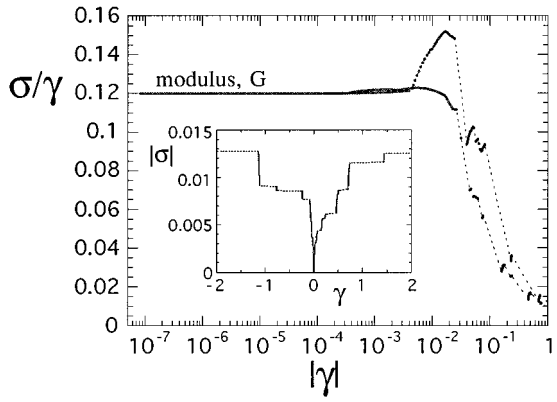

FIG. 6. The strain γ at which mechanical equilibrium is achieved with the imposed stress σ, for a 12×12 system of bubbles with gas fraction $\phi=1$ and distribution width $w=0.75$. Data points were obtained by successively increasing σ from zero, in both positive and negative directions, and recording the strain once static equilibrium was reestablished. Irreversible slips, where a large motion was caused by a small stress increment, are denoted by dashed lines.

strains throughout the range $0<|\gamma|<0.03$ can be achieved by suitable choice of applied stress, and the motion is fully reversible; for example, if the applied stress is set to zero then the system will relax back to a strain of zero. Beyond this point, however, a small increment in stress can produce a dramatically large, irreversible, increase in strain. As the applied stress passes a threshold, the strain in some region of the foam becomes so large that a pair, or pairs, of bubbles are pushed past one another; when this occurs, their repulsive interactions no longer counteract the applied shear but in fact aid it. Flow thus ensues, and the spring network rearranges until a stiffer bubble configuration arises that is able to support the higher level of applied stress. The strain thus advances considerably at nearly the same stress, as shown by the dashed lines in Fig. 6 between points of static mechanical equilibrium. Note that once flow has occurred, the motion can no longer be reversed: cessation of applied shear will not result in a return to zero strain. New configurations of mechanical stability, in turn, eventually give way as the applied stress is further increased. Finally, the applied stress becomes too great to support any bubble arrangement, and the system flows indefinitely. For the example foam studied in Fig. 6, the largest static strains observed are between 1 and 1.5 in magnitude; the simulation was stopped when the flow exceeded a strain of 10 under the assumption that static mechanical equilibrium would never again be achieved. The corresponding yield stress required to produce indefinite flow is slightly less than 0.013, comparable to the shear modulus. It is worth emphasizing that the onset of irreversibility, where topological rearrangements first occur, is nearly two orders of magnitude below this point.

The behavior during indefinite flow can be studied under conditions of constant applied stress, but not easily since the strain rate is fairly constant only when the stress is much greater than the yield stress. As the yield stress is approached from above, the motion becomes increasingly nonuniform, slowing down as stiff bubble arrangements arise and speeding up as they are broken. Very long runs are then needed to ascertain the average strain rate, which will vary dramatically very close to the yield stress. This can be seen clearly in the following simple physical picture of the dynamics. Suppose in static mechanical equilibrium that the stress increases linearly with strain all the way up to the yield point, drops immediately to zero, and then repeats periodically. The shear modulus is then given by the yield stress and yield strain as $G=\sigma_y/\gamma_y$. The equation of motion for the strain as a function of time in response to a given applied stress σ_y is then

$$0=\sigma_A-G\gamma-\mu d\gamma/dt, \tag{6}$$

where μ is the so-called plastic viscosity of the system, since the applied, elastic, and viscous forces must sum to zero. This equation can be transformed into the empirical Bingham plastic relation found for actual foams [4,5] simply by replacing the elastic $G\gamma$ term by the yield stress, as though in a random foam the elastic stress is always at the yield point, and by assuming that the strain rate is constant in time. For a periodic foam, Eq. (6) can be integrated over one strain cycle to obtain the period, which in turn gives the average strain rate as

$$\langle\dot{\gamma}\rangle=-\frac{\sigma_y}{\mu\,\ln[1-\sigma_y/\sigma_A]}. \tag{7}$$

In the limit of very large applied stress, $\sigma_A\gg\sigma_y$, the elastic $G\gamma$ term in Eq. (6) is negligible and Eq. (7) predicts a viscous response at nearly uniform rate, $\langle\dot{\gamma}\rangle\to\sigma_A/\mu$. As the stress is lowered, the average strain rate decreases and an increasingly greater fraction of the strain cycle is spent creeping up to the yield strain. To produce arbitrarily small strain rates, the applied stress must be made infinitesimally greater than the yield stress. In constant-stress computer simulations this is difficult because the yield stress is not known in advance and is difficult to locate accurately, as seen in Fig. 6. A practical solution might be to simulate a system with large enough aspect ratio that the strain rate becomes uniform, never deviating far from the average value.

VI. STEADY STRAIN-RATE RESULTS

Rather than simulate flow behavior under conditions of constant applied stress, it is simpler to impose constant strain-rate conditions and then characterize the resulting time-dependent stresses. The behavior under steady strain-rate flow is the subject of the remainder of this paper. After thorough equilibration, the simulations thus proceed by a series of small time steps in which the top and bottom edge walls are translated according to the desired strain rate while the bulk bubbles are simultaneously allowed to move according to Eq. (3), with $\langle\vec{v}_j\rangle=\dot{\gamma}y_i\hat{x}$.

A. Bingham-plastic behavior

Results for a 6×6 system were shown previously in Ref. [35]. Here, analogous results for a single 12×12 system with gas fraction $\phi=1$ are shown in Fig. 7, always for the same initial equilibrated bubble configuration. The inset depicts raw data for the shear stress on the walls as a function of strain for several different strain rates, labeled according to

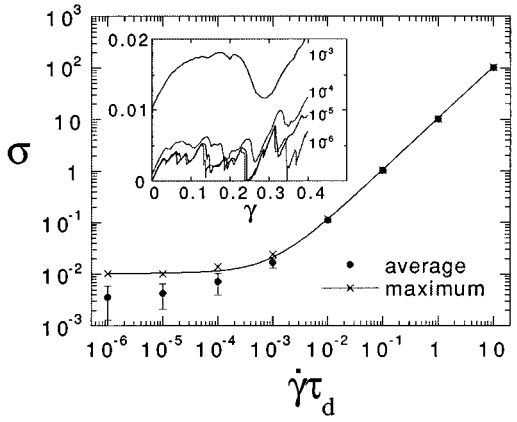

FIG. 7. Average and maximum shear stress vs imposed strain rate, $\dot{\gamma}\tau_d$, for a 12×12 system of bubbles with gas fraction $\phi=1$ and distribution width $w=0.75$. Error bars denote rms fluctuations about the average, and the solid curve is a fit of the maximum to Bingham-plastic behavior. Raw stress vs strain data are shown in the inset for several dimensionless strain rates as labeled.

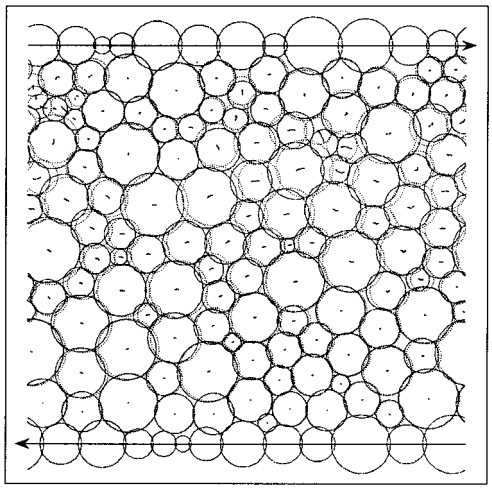

FIG. 8. Bubble configurations before (dotted circles) and after (solid circles) a sudden topological rearrangement that occurred at an infinitesimal strain rate of $\dot{\gamma}\tau_d=10^{-5}$; bubble-center trajectories are also shown. This particular event released more elastic energy from the spring network than any other observed in the 12×12 simulation run; nevertheless, the topology change involved only a few bubbles.

Deborah number, $\dot{\gamma}\tau_d$, where $\tau_d=b\langle R\rangle/F_0$ is the microscopic relaxation time constant defined earlier. In all cases, the stress initially increases and then undergoes a series of fluctuations about some well-defined average. As the strain rate is increased, the inset shows how the average level of shear stress also increases while the frequency and relative size of the stress fluctuations decrease. Such behavior is summarized in the main plot by the average and maximum stress, tabulated over the range $0<\gamma<10$, versus Deborah number; error bars denote the rms size of fluctuations about the average, not statistical uncertainty. As the strain rate increases, the relative size of the fluctuations is clearly seen to shrink while the maximum eventually becomes indistinguishable from the average. In the opposite direction, as the strain rate decreases, the stress versus strain and strain rate approach a limiting behavior, as seen both in the inset and in the leveling off of the maximum and average in the main plot.

Physically, the simulated stress versus strain and strain rate behavior depicted in Fig. 7 can be understood as follows. First, at high strain rates, the viscous dissipation term $\langle\vec{v}_j\rangle=\dot{\gamma}y_i\hat{x}$ in Eq. (3) is much larger than the repulsive spring interactions. Accordingly, the instantaneous velocity of each bulk bubble approaches the average value of all its neighbors, $\vec{v}_i\rightarrow\langle\vec{v}_j\rangle=\dot{\gamma}y_i\hat{x}$, and the deformation of the system becomes affine. In this limit, where the source of elasticity is negligible, the response of the foam is exactly like that for a purely viscous liquid undergoing shear. In the opposite limit, of very small strain rates, the viscous interactions in Eq. (3) are essentially negligible and the bubble configuration is therefore almost always in mechanical equilibrium with the applied shear forces. Thus, the stress versus strain rate approaches a limiting behavior that is independent of strain rate. The source of fluctuations is, of course, the irreversible rearrangement of bubbles from one tightly packed configuration to another. As seen in the inset of Fig. 7, and also in the constant-stress simulation results of Fig. 6, this first occurs at a strain of around 3%. An example of such a rearrangement is shown in Fig. 8 and will be discussed in detail later; for now, note only that viscous interactions cannot be ignored during rearrangement, even though they are otherwise negligible at low strain rates, and that the fastest time scale in the rearrangement motion is set by τ_d. The characteristic time scale that separates the low strain rate behavior from the viscous high strain rate behavior is ultimately also set by this microscopic time, τ_d. The former regime is achieved only when rearrangements are discrete and come to completion before noticeable macroscopic shear occurs, and the latter regime is achieved only when rearrangements are induced at such a high rate that they merge together into continuous uniform motion.

The simulation results shown in Fig. 7 can be compared quantitatively with expectations for real foams. Experience [3–5] shows that the typical stress versus strain rate relationship is roughly that of a Bingham plastic, $\sigma=\sigma_y+\mu_p\dot{\gamma}$. A reasonably good fit of this form to the maximum stress data is shown in Fig. 7, where the yield stress is $\sigma_y=0.01$ and plastic viscosity is $\mu_p=10\tau_d$. As found previously [35], the plastic viscosity is set by the stress relaxation time and confirms the above expectation regarding the crossover time scale. Note that the rise of the maximum stress data away from the low strain rate limit is slightly more gradual than the Bingham plastic form, and is significantly more gradual for the average stress data. The prediction of Eq. (7) is even worse in this respect. This is not a crucial issue, however, since real foams are nonequilibrium systems that are able to relax elastic stresses via time evolution, causing the stress to drop to zero for very small strain rates. The important point is that the model presented here for bubble dynamics in a flowing foam successfully reproduces the apparent Bingham-plastic behavior seen for real foams at strain rates large in comparison with evolution time scales. The only other simulations that include dissipation effects to achieve finite rates of shear are of Kawasaki's vertex model, in which the viscous force between two vertices scales as their relative velocity raised to the power of $\frac{2}{3}$ [28–30]. This model also produces results consistent with Bingham-plastic behavior for stresses slightly larger than the yield stress. However, for

TABLE I. Rearrangement event statistics at a uniform imposed strain rate $\dot{\gamma}\tau_d = 10^{-5}$ and gas fraction $\phi = 1$. The number of bubbles is $N \times N$, with the top and bottom N bubbles fixed to the edge plates, and the total shear strain suffered during the run is γ_m. The resulting number of events is N_e; the event rate expressed as the number per bulk bubble per unit strain is $R_e = N_e/(N^2 - 2N)\gamma_m$; the average energy release in units of the average bubble energy is $\langle \Delta E \rangle / E_b$, with standard deviation as given; and the median energy release in units of the average bubble energy is $\Delta E_m / E_b$.

N	γ_m	N_e	R_e	$\langle \Delta E \rangle / E_b$	Standard dev.	$\Delta E_m / E_b$
6	116	1510	0.542	1.77	2.49	0.469
12	40.0	1763	0.376	2.22	3.45	0.510
18	22.8	1953	0.297	2.36	3.89	0.554
30	11.2	2050	0.218	2.41	4.22	0.550

very large strain rates where viscous forces completely dominate, it is hard to see how stress could be proportional to strain rate when the viscous force between neighbors is assumed not to be proportional to their velocity difference.

B. Avalanches

Attention is finally turned to the nature of the sudden avalanchelike topological rearrangements that occur when a foam is sheared slowly. This has been simulated previously by Okuzono and Kawasaki using their vertex model for a perfectly dry, two-dimensional system of over 1000 bubbles contained in a square cell and subjected to shear at dimensionless rate of 10^{-4} [30]. They measure the size of each rearrangement event by the drop in total elastic energy triggered unexpectedly by a small increment in strain. A broad spectrum of events is found, such that the probability of occurrence decreases as a power law of size with an exponent of $-\frac{3}{2}$. This was based on almost 10 000 events spread over a total strain increase of 20, giving an average of about 0.5 event per bubble per unit strain. Such behavior is claimed to be a deterministic example of self-organized criticality in which events, or avalanches, occur in all sizes ranging from a few bubbles to all in the system. This is supported by figures showing large-scale circulatory flows that suddenly start then stop. Avalanche statistics have also been reported by Hutzler, Weaire, and Bolton for a two-dimensional system of 50 bubbles subjected to quasistatic extension [27]. Rather than tabulate energy drops, they measure avalanche size by the number of changes in nearest-neighbor contacts that must be performed simultaneously in order to restore mechanical equilibrium. Histograms for this number are sharply peaked for dry foams, but become broader and appear to develop a power-law tail with exponent of -1 as the liquid content increases toward the melting point. It is not clear how to reconcile these two sets of observations given the significant differences in the models, in the quantities tabulated, and in system sizes and the level of statistics. A consistent qualitative feature, however, is that the flow of foam is accomplished intermittently by a series of sudden avalanchelike topological rearrangement events with a broad distribution of sizes, seemingly consistent with self-organized criticality.

Experimentally, the sudden rearrangement events induced in a slowly sheared three-dimensional foam with gas fraction 0.92 have been observed recently by Gopal and myself using diffusing-wave spectroscopy, a noninvasive multiple-light-scattering technique [9]. We find that macroscopically homogeneous shear deformation is accomplished by sudden localized rearrangement events, without noticeable accumulation of affine shear strain. We also find that the distribution for the number of bubbles involved per avalanche must be peaked, with no power-law tail; it has a well-defined average corresponding to a small region roughly four bubbles across, and is independent of system size. This is completely inconsistent with the picture of self-organized criticality suggested in Refs. [27, 30].

To begin reconciling theory and experiment, it is useful to examine the nature of rearrangements predicted by the bubble model for foam mechanics. This is simply a matter of extending and analyzing the simulations used to produce Fig. 7. Like Kawasaki's vertex model, the bubble model has the virtue of including dissipation effects to produce rearrangements with realistic dynamics and finite duration. But, since bubble motion occurs entirely according to Eq. (3), it has an advantage over both the Kawasaki and Weaire approaches in that topology need not be separately monitored and updated ''by hand'' when a film shrinks to zero length. Simulations are thus performed as above for several square systems of bubbles, each with gas fraction $\phi = 1$, subjected to shear at a constant rate of $\dot{\gamma}\tau_d = 10^{-5}$. As seen from Fig. 7, this is slow enough to obtain the low strain rate limiting behavior. There, rearrangement events are evident as the sudden drops in stress that come after a gradual rise. The motion involved in such an event is depicted in Fig. 8 by the bubble locations both before and after the stress drop, along with the center positions at all times in between. The sudden avalanchelike nature of this event is apparent from the large scale of motion in the interior, ranging up to about one bubble diameter, and the infinitesimal motion of the edge walls throughout its duration. Note that the event in Fig. 8 involves two compact clusters of bubbles undergoing topology change, in the upper left and upper middle right. Surrounding these two clusters is a large swath of bubbles that shift without neighbor change more or less coherently, though with gradually decreasing amplitude.

Following Okuzono and Kawasaki [30], avalanches can usefully be described by the elastic energy drop per event. The extent of the runs and the resulting event statistics are given in Table I. In comparison with Okuzono and Kawasaki, the system sizes range from significantly to slightly smaller, but the runs are typically longer. Results for the average event rate decrease somewhat with system size, and extrapolate linearly to about 0.15 per bulk bubble per unit strain as $1/N$ goes to zero. Note that since the largest system simulated here is significantly closer to this limit than the smallest, the effects of the finite sample size do not dominate

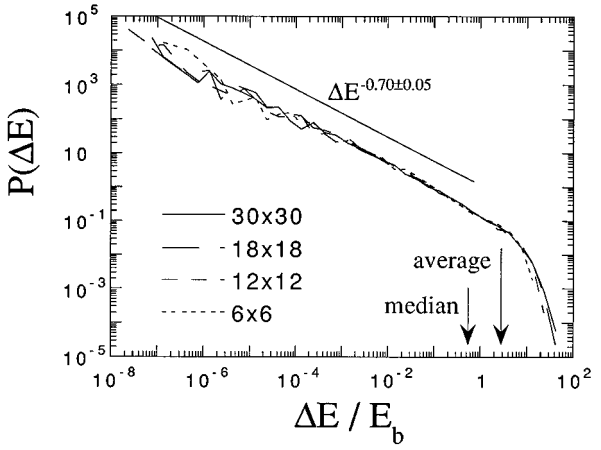

FIG. 9. Probability density for rearrangement events releasing energy ΔE, normalized by the average energy per bubble E_b. Details of the simulation runs are given in Table I. Independent of system size (labeled), there is a preponderance of small events exhibiting power-law behavior, with exponent 0.70 ± 0.05, and an exponential cutoff of large events.

behavior; this can also be seen in the other event statistics in Table I. The average rearrangement rate is only slightly larger in the Okuzono-Kawasaki simulations, 0.50 per bubble per unit strain.

While event rates may be comparable, the nature of the flows and the quantitative details of the probability density, $P(\Delta E)$, for events with energy drop ΔE, are entirely different for the bubble and vertex models. Figure 9 shows this distribution based on the simulation runs summarized in Table I. Results for the four system sizes are nearly indistinguishable, as seen already in Table I, and adequately represent the infinite-sample limit. Evidently, the range of energy drops produced by the bubble model spans an enormous range, from 10^{-7} to 50 times the average bubble energy, E_b. The preponderance of events is small, with the median size being about $0.6E_b$ and the average being about $2.5E_b$. For small events, below this average, the distribution is a power law with exponent -0.70 ± 0.05; for large events, it decays as $\exp(-0.2\Delta E/E_b)$. Without this exponential cutoff, the average and width of the distribution reported in Table I would not be well defined. This contrasts with the Okuzono-Kawasaki vertex model simulations [30], where energy drops occur over only two decades, in spite of the larger system, and where the distribution is a power law, $P(\Delta E)\propto\Delta E^{-3/2}$. Not only is their exponent different, but they find no sign of an exponential cutoff for large events. A related difference is that the largest events in the vertex model presumably depend on system size, but do not in the bubble model.

The avalanche statistics of the bubble model, though in conflict with those of the vertex model, are actually in good accord with the experiments by Gopal and myself [9]. Both show lack of a power-law tail in the distribution of large events, which leads to a well-defined average event size. And both show that the average event is relatively small, only a few bubbles across. For the bubble model, this can be seen two ways. First, most events are smaller than the average bubble energy E_b and are exponentially rare above $5E_b$. Second, and perhaps more significantly, the extent of bubble motion is not very large. For example, the event motion shown in Fig. 8 is actually atypical; it is for the *largest* energy drop seen in the 12×12 system. Even for this largest of events, the clusters of bubbles undergoing topology change only involve a few bubbles, and the individual motions are not more than a typical bubble size. Work is now in progress [42] to determine whether the choice of dissipative dynamics in Eq. (3) plays a role in forcing the typical event size to be commensurate with the bubble size.

Physically, the cause for better agreement with experiment may be that the bubbles are less constrained and hence can rearrange before being significantly distorted. In both experiment and bubble model, rearrangements can be induced by strains of only a few percent; as more strain is imposed, the bubbles simply rearrange to maintain shapes fairly close to equilibrium. Accordingly, the elastic energy is never much higher than in unstrained equilibrium and the magnitude of the stress fluctuations is comparable to the average, as seen in Fig. 7. In the vertex model, by contrast, rearrangements are not induced until the bubbles are very highly distorted and the strains exceed 1; as more strain is imposed, rearrangements occur but only relieve a small portion of the extra energy, leaving the bubbles still highly distorted. Accordingly, the elastic energy is significantly higher than in unstrained equilibrium and the stress fluctuations are small compared to the average, as seen in Figs. 3 and 4 of Ref. [30]. This ''loading'' produced in the vertex model may be the crucial difference. It does not occur in the bubble model, presumably because the bubbles are always spherical and the corresponding repulsive springs cannot be significantly compressed via shear. It does not occur in experiment either, presumably because bubbles are harder to constrain for a foam which is fairly wet and which exists in three dimensions.

ACKNOWLEDGMENTS

Helpful conversations with R. Bruinsma, K. Kawasaki, S. A. Langer, A. J. Liu, S. Ramaswamy, and D. A. Weitz are gratefully acknowledged. This work was partially supported by NASA Grant No. NAG3-1419.

[1] J. H. Aubert, A. M. Kraynik, and P. B. Rand, Sci. Am. **254**, 74 (1989).

[2] D. J. Durian and D. A. Weitz, in *Kirk-Othmer Encyclopedia of Chemical Technology*, edited by J. I. Kroschwitz (Wiley, New York, 1994), Vol. 11, p. 783.

[3] G. R. Assar and R. W. Burley, in *Gas-Liquid Flows*, edited by N. P. Cheremisinoff (Gulf Publishing Company, Houston, 1986), Vol. 3, p. 26.

[4] J. P. Heller and M. S. Kuntamukkula, Ind. Eng. Chem. Res. **26**, 318 (1987).

[5] A. M. Kraynik, Annu. Rev. Fluid Mech. **20**, 325 (1988).
[6] D. J. Durian, D. A. Weitz, and D. J. Pine, Science **252**, 686 (1991).
[7] J. C. Earnshaw and A. H. Jafaar, Phys. Rev. E **49**, 5408 (1994).
[8] J. C. Earnshaw and M. Wilson, J. Phys. Condens. Matter **7**, L49 (1995).
[9] A. D. Gopal and D. J. Durian, Phys. Rev. Lett. **75**, 2610 (1995).
[10] J. C. Earnshaw and M. Wilson, J. Phys. (France) II **6**, 713 (1996).
[11] A. D. Gopal and D. J. Durian, J. Opt. Soc. Am. A **14**, 150 (1997).
[12] R. K. Prud'homme, Ann. Meet. Soc. Rheol., Louisville, KY, 1981 (unpublished).
[13] H. M. Princen, J. Col. I. Sci. **91**, 160 (1983).
[14] A. J. Liu, S. Ramaswamy. T. Mason, H. Gang, and D. A. Weitz, Phys. Rev. Lett. **76**, 3017 (1996).
[15] D. Weaire and J. P. Kermode, Philos. Mag. B **48**, 245 (1983).
[16] D. Weaire and J. P. Kermode, Philos. Mag. B **50**, 379 (1984).
[17] T. Herdtle and H. Aref, J. Fluid Mech. **241**, 233 (1992).
[18] D. Weaire, F. Bolton, T. Herdtle, and H. Aref, Philos. Mag. Lett. **66**, 293 (1992).
[19] K. A. Brakke, Expt. Math. **1**, 141 (1992).
[20] D. Weaire and R. Phelan, Philos. Mag. Lett. **69**, 107 (1994).
[21] D. A. Reinelt and A. M. Kraynik, J. Fluid Mech **331**, 327 (1996).
[22] A. M. Kraynik (private communication).
[23] F. Bolton and D. Weaire, Phys. Rev. Lett. **65**, 3449 (1990).
[24] F. Bolton and D. Weaire, Philos. Mag. B **63**, 795 (1991).
[25] F. Bolton and D. Weaire, Philos. Mag. B **65**, 473 (1992).
[26] S. Hutzler and D. Weaire, J. Phys. Condens. Matter **7**, L657 (1995).
[27] S. Hutzler, D. Weaire, and F. Bolton, Philos. Mag. B **71**, 277 (1995).
[28] K. Kawasaki, T. Okuzono, and T. Nagai, J. Mech. Behav. Mat. **4**, 51 (1992).
[29] T. Okuzono and K. Kawasaki, J. Rheol. **37**, 571 (1993).
[30] T. Okuzono and K. Kawasaki, Phys. Rev. E **51**, 1246 (1995).
[31] *Thin Liquid Films: Fundamentals and Applications*, Vol. 29, edited by I. B. Ivanov (Marcel Dekker, New York, 1988).
[32] A. W. Adamson, *Physical Chemistry of Surfaces* (John Wiley & Sons, New York, 1990).
[33] D. M. A. Buzza, C. Y. D. Lu, and M. E. Cates, J. Phys. (France) II **5**, 37 (1995).
[34] W. Schwartz and H. M. Princen, J. Colloid Interface Sci. **118**, 201 (1987).
[35] D. J. Durian, Phys. Rev. Lett. **75**, 4780 (1995).
[36] M.-D. Lacasse, G. S. Grest, D. Levine, T. G. Mason, and D. A. Weitz, Phys. Rev. Lett. **76**, 3448 (1996).
[37] D. C. Morse and T. A. Witten, Europhys. Lett. **22**, 549 (1993).
[38] T. G. Mason, J. Bibette, and D. A. Weitz, Phys. Rev. Lett. **75**, 2051 (1995).
[39] M.-D. Lacasse, G. S. Grest, and E. Levine, Phys. Rev. E **54**, 5436 (1996).
[40] M. P. Allen and D. J. Tildesley, *Computer Simulation of Liquids* (Oxford University Press, New York, 1992).
[41] W. H. Press, B. P. Flannery, S. A. Teukolsky, and W. T. Vetterling, *Numerical Recipes in C* (Cambridge University Press, New York, 1988).
[42] S. A. Langer (private communication).
[43] H. M. Princen, J. Colloid Interface Sci. **71**, 55 (1979).
[44] D. Bideau and J. P. Troadec, J. Phys. C **17**, L731 (1984).
[45] S. Feng, M. F. Thorpe, and E. Garboczi, Phys. Rev. B **31**, 276 (1985).